




Article

Precipitation Climatology for the Arid Region of the Arabian Peninsula—Variability, Trends and Extremes

Platon Patlakas ^{1,2}, Christos Stathopoulos ^{1,2}, Helena Flocas ¹, Nikolaos S. Bartsotas ^{1,2}
and George Kallos ^{1,2,*}

¹ Department of Physics, National and Kapodistrian University of Athens, University Campus, Bldg. PHYS-V, 15784 Athens, Greece; platon@mg.uoa.gr (P.P.); chrisstath@mg.uoa.gr (C.S.); efloca@phys.uoa.gr (H.F.); nikos@mg.uoa.gr (N.S.B.)

² Weather & Marine Engineering Technologies P.C. (WeMET P.C.), 17456 Athens, Greece

* Correspondence: kallos@mg.uoa.gr

Abstract: The Arabian Peninsula is a region characterized by diverse climatic conditions due to its location and geomorphological characteristics. Its precipitation patterns are characterized by very low annual amounts with great seasonal and spatial variability. Moreover, extreme events often lead to flooding and pose threat to human life and activities. Towards a better understanding of the spatiotemporal features of precipitation in the region, a thirty-year (1986–2015) climatic analysis has been prepared with the aid of the state-of-the-art numerical modeling system RAMS/ICLAMS. Its two-way interactive nesting capabilities, explicit cloud microphysical schemes with seven categories of hydrometeors and the ability to handle dust aerosols as predictive quantities are significant advantages over an area where dust is a dominant factor. An extended evaluation based on in situ measurements and satellite records revealed a good model behavior. The analysis was performed in three main components; the mean climatic characteristics, the rainfall trends and the extreme cases. The extremes are analyzed under the principles of the extreme value theory, focusing not only on the duration but also on the intensity of the events. The annual and monthly rainfall patterns are investigated and discussed. The spatial distribution of the precipitation trends revealed insignificant percentage differences in the examined period. Furthermore, it was demonstrated that the eastern part and the top half of the western Arabian Peninsula presented the lowest risk associated with extreme events. Apart from the pure scientific interest, the present study provides useful information for different sectors of society and economy, such as civil protection, constructions and reinsurance.

Keywords: regional climatology; precipitation; rainfall; Arabian Peninsula; arid/semi-arid region precipitation; dynamical downscaling; trend analysis; extremes; intensity duration frequency; return periods



Citation: Patlakas, P.; Stathopoulos, C.; Flocas, H.; Bartsotas, N.S.; Kallos, G. Precipitation Climatology for the Arid Region of the Arabian Peninsula—Variability, Trends and Extremes. *Climate* **2021**, *9*, 103. <https://doi.org/10.3390/cli9070103>

Academic Editor: Mário Gonzalez Pereira

Received: 5 May 2021

Accepted: 16 June 2021

Published: 22 June 2021

Publisher's Note: MDPI stays neutral with regard to jurisdictional claims in published maps and institutional affiliations.



Copyright: © 2021 by the authors. Licensee MDPI, Basel, Switzerland. This article is an open access article distributed under the terms and conditions of the Creative Commons Attribution (CC BY) license (<https://creativecommons.org/licenses/by/4.0/>).

1. Introduction

The climate of the Arabian Peninsula (AP) is affected by the Indian monsoon in the south and the Mediterranean synoptic scale systems in the north. Furthermore, the complex landscape—consisting of highlands in the western and southwestern regions, vast arid and extra arid lands in the mainland, the Red Sea in the west and the sand desert in the southeast—plays an important role in the formation of the regional climatic features. The topography in Saudi Arabia varies from low altitudes in the coastal areas (0 up to 100 m) to high altitudes in the mountainous areas (more than 2000 m).

The precipitation regime of the AP is generally characterized by arid climatological characteristics. Limited and infrequent rainfall events occur mainly from October through April [1], except for the southwestern region, where high precipitation amounts are reported [2]. However, precipitation is not extensively analyzed due to its irregularity in space and time and the sparseness and/or unavailability of long records of observational datasets.

Almazroui et al. [3,4] investigated the annual and seasonal distribution of precipitation along with trends, employing station data and gridded datasets for the period 1979–2009. Alsarmi and Washington [5] calculated trends of precipitation in AP using also station data. Barth and Steinkohl [6] investigated the role of synoptic scale systems on winter precipitation of AP and demonstrated the role of Mediterranean depressions, the Sudan low and convective systems. The climatological characteristics and mechanisms of rainfall in AP are reviewed by Hasanean and Almazroui [1]. Mahmoud et al. [7] evaluated the seasonal rainfall and rainfall intensity in Saudi Arabia as derived from the satellite IMERG products against station measurements.

Extreme precipitation events commonly occur in AP throughout the whole year due to the deep convection triggered by tropical and extratropical forcing along with the orography [8]. These extreme events frequently cause floods with severe impacts on human life and economy. It is worth mentioning that the extreme daily precipitation events contribute to about 20–70% of the total precipitation over the AP [9].

Regional climatic patterns of temperature, relative humidity and wind in the AP were studied by Patlakas et al. [10] with the aid of a state-of-the-art, limited area atmospheric modeling system. More precisely, the employment of a high resolution atmospheric model resolved the problem of limited or unavailable data in particular areas and provided an insight on complicated climatic features. The atmospheric model simulated the spatial and temporal variations of the above mentioned climatic parameters over AP with a more reliable and detailed behavior, when compared to previous results of regional climatic models.

As a further attempt to extend the study of Patlakas et al. [10], this work aims to present a regional precipitation climatology for the AP, employing the regional atmospheric model RAMS/ICLAMS. The model has run for a 30-year period (1986–2015) with a spatial resolution of 9 km and a temporal resolution of 3 hours. The great advantages of adopting RAMS/ICLAMS for a study focusing on precipitation are its highly sophisticated physical parameterizations, including dust and its numerical schemes, allowing the depiction of local scale patterns that are not represented in the simulations of climatic models. More specifically, the objectives are: a) to investigate the spatial precipitation patterns in the AP on a monthly basis, aiming to better assess the spatial and temporal variation of precipitation b) to examine the precipitation extremes along with their characteristics, such as intensity, duration and return periods and c) to analyze the precipitation trends in the AP for a period of 30 years (1986–2015).

2. Materials and Methods

2.1. Intensity, Duration and Frequency of Rainfall Events

The probability of the average rainfall intensity over given periods of time can be expressed under the principles of the Extreme Value Theory and depicted employing rainfall Intensity–Duration–Frequency (IDF) curves [11]. These are used to estimate the relationship between a precipitation event and its frequency in terms of return periods. Extreme cases derived from the IDF curves are adopted, among others, by hydrometeorologists, engineers and civil protection agencies for the design of urban drainage systems and the assessment of regional flood vulnerabilities [12,13].

According to Koutsoyiannis et al. [14], a basic step towards their construction is the retrieval of extreme rainfall intensities for different durations through an annual maximum analysis. These annual maximum values (Annual Maxima—AM) are well represented by different theoretical distribution functions. Among the most common procedures is to fit the Generalized Extreme Value distribution (GEVd) to the created subset and retrieve the estimated fitted parameters for each selected duration. These parameters will be used for the estimation of the reoccurrence intervals and lead to the relation between the intensity, duration and frequency and subsequently to the creation of the IDF curves.

In this study, the annual maximum rainfall rate values for the 30-year period and for each model grid were obtained. These maximum rain rate values were determined for

different accumulation periods: 3 h to 48 h with a 3-h interval. The AM are often well approached by the first type of the GEVd [15,16]. Therefore, the Gumbel distribution is selected since only two parameters are required [17]. The estimation of the parameters is performed based on the Maximum Likelihood (ML) method [18,19]. The scale and the location parameter (α and β , respectively) can be estimated through the simultaneous numerical solution of the following equations:

$$\tilde{x} - \frac{\sum_{t=1}^n x_t \exp(-x_t/a)}{\sum_{t=1}^n \exp(-x_t/a)} - a = 0 \text{ and } -a \cdot \log\left[\frac{1}{n} \sum_{i=1}^n \exp\left(-\frac{x_i}{a}\right)\right] - \beta = 0 \quad (1)$$

where x_1, \dots, x_n is a random sample and \tilde{x} is the sample mean.

The estimation of the design values/intensities (I_T) for a preferred return period (T) is performed through the relation between the cumulative frequency (F) and T [16]:

$$F(I_T) = 1 - (1/T) \quad (2)$$

Substituting the cumulative distribution function (CDF) of Gumbel, transforms Equation (2) to the following:

$$I_T = \beta - \alpha \ln[-\ln(1 - 1/T)] \quad (3)$$

The procedure was followed for return periods set to 10, 25, 50, 75 and 100 years.

More details and applications on IDF curves can be found in the following publications [20–24].

2.2. Data, Model Set up and Evaluation Metrics

The data used for the analysis of the precipitation characteristics is the product of dynamical downscaling based on a regional atmospheric modeling system. The model used is the Integrated Community Limited Area Modeling System (ICLAMS) based on the Regional Atmospheric Modeling System (RAMSv6) [25,26]. RAMS/ICLAMS was developed within the Atmospheric Modeling and Weather Forecasting Group (AM&WFG) of the University of Athens, Greece [10,27–31]. It has two-way interactive nesting capabilities, an explicit cloud microphysical scheme with seven categories of hydrometeors and the ability to handle dust aerosols as predictive quantities. Concentrations, size distributions and optical properties of all elements are computed online. Natural aerosols contribute to the calculation of the meteorological conditions through feedback mechanisms (direct, semi-direct and indirect effects). The aforementioned features render the use of the model as most appropriate, especially over an area where dust is a dominant factor.

The simulation period covers the years between 1986 and 2015 (30 years). The model spatial resolution is 9 km and the corresponding timestep is 15 seconds. The domain extent (Figure 1) has a significant buffer zone around the Arabian Peninsula so that the boundaries would not affect the study area. Vertically, it stretches up to 20 km with 30 levels, while the output is saved every 3 hours.

ERA-Interim [32] data is employed for the regional model initial and boundary conditions. This dataset is a global atmospheric reanalysis product distributed by the European Centre for Medium-Range Weather Forecasts (ECMWF) beginning from 1979. A major advantage in the use of such products for climatological studies is the consistency, homogeneity and robustness in terms of model outputs.

For Sea Surface Temperature (SST), the high resolution 0.083-deg analyses from NCEP have been used [33]. The soil texture and properties within the boundaries of the Kingdom of Saudi Arabia are derived from a custom soil categorization dataset, based on a very high resolution soil database from Saudi Aramco. Soil data for the neighboring countries originate from the Food and Agriculture Organization of the United Nations (FAO). The geological categories were grouped into several soil textural categories based upon their common properties. Vegetation and land use were acquired by USGS following the Olson

the Tropical Rainfall Measuring Mission (TRMM) and Global Precipitation Measurement (GPM) retrievals [38]. Version 6 of the final product that is used in this study is an outcome of the combination, filtering and interpolation of all available passive microwave precipitation estimates, microwave-calibrated infrared (IR) satellite estimates and calibration from available precipitation gauges [39]. It is provided in a resolution of 0.1×0.1 , every thirty minutes starting from 2000.

In particular, the comparison concerns the mean annual accumulated precipitation, illustrated in Figure 2 (the mean monthly accumulated precipitation -IMERG- can be found in Appendix A). Cumulatively, the spatial distribution of rainfall between modeled and remote sensing estimates is in an acceptable agreement. Both modeled and satellite outputs demonstrate the low and moderate precipitation fields that dominate the northwest and southeast regions of the Peninsula. Likewise, the increased precipitation rates emerging in the north due to the cyclonic activity of the Mediterranean Sea and in the east parts of the Africa are evident in both products. Differences are noticed over the Red Sea, where modeled precipitation presents higher magnitudes. This can be associated with the complex processes prevailing in the current area including the seasonal variations and the intense convective activity. Furthermore, the absence of rain gauge data over ocean, which effectively adjusts the satellite precipitation estimates over land, might also have contributed towards a notable underestimation from IMERG over this area. Similar conclusions are reached upon comparison of the mean monthly accumulated precipitation (Figure 8 and Figure A1).

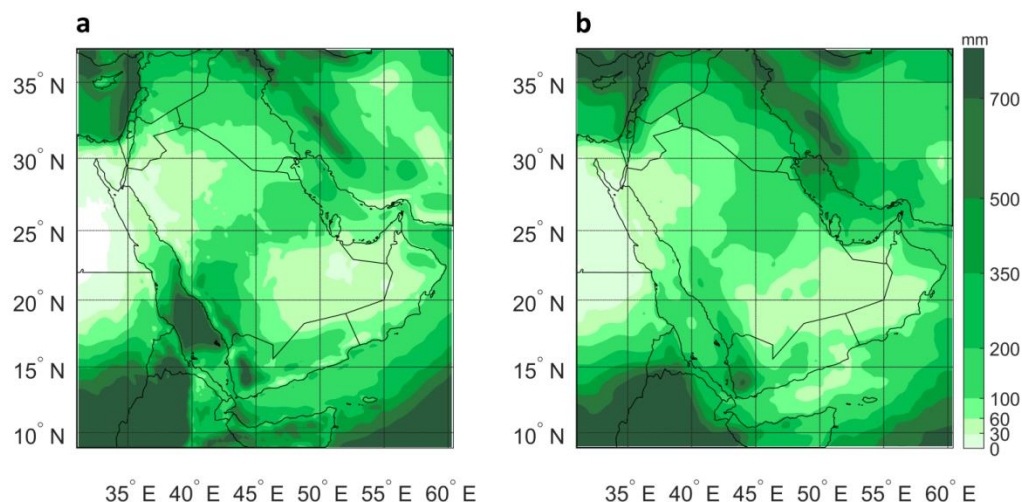


Figure 2. Mean annual accumulated precipitation of (a) the model output and (b) the IMERG product for the years 2001–2015.

The NWP evaluation against station data was carried out with the use of different weights from the four nearest model grid points based on the distance from the station. This approach is considered as conventional for the provision of model outputs over a specific location and partly counterbalances the high spatiotemporal variability of precipitation.

Precipitation measurements were employed from a network of meteorological stations operating in the peninsula. These are in accordance with the World Meteorological Organization (WMO) requirements, updated on daily basis [40] in 3-h intervals. 22 stations were used in the current study, primarily based on data availability and sufficient area coverage, for the whole 30-year period of the model simulations. At this point, it should be noted that the rain gauge data in the area are sparse and most of the precipitation events are of convective type, making the evaluation procedure rather difficult.

The MBE results for the whole period fall within the range -0.2 and 0.2 mm, with the vast majority being restrained within the -0.1 and 0.1 mm margins (Figure 3a). Concurrently, the mean errors are almost equally distributed positively and negatively around zero. As a result, a concrete conclusion for a tendency of a systematic overestimation or

underestimation in the model results cannot be extracted. Most of the RMSE values are traced between the 1 mm and 2 mm of rainfall.

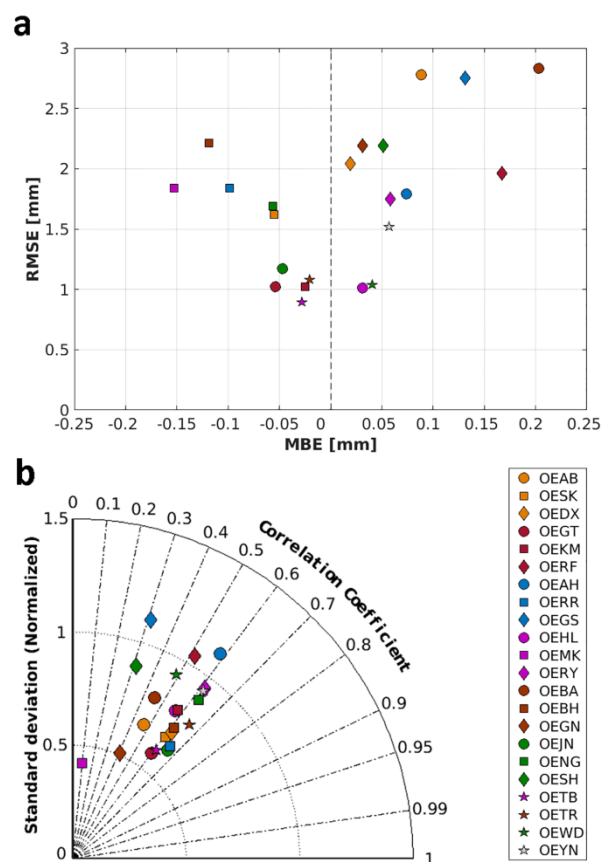


Figure 3. (a) MBE versus RMSE between modeled and observed precipitations and (b) Taylor diagram for each station.

Additional statistical information is provided by the Taylor diagram (Figure 3b), illustrating the correlation coefficient values together with the normalized standard deviations (the ratio between modeled standard deviation and the observed one). Modeled and measured precipitation values are positively correlated with most of the coefficient values found between 0.4 and 0.7. Overall, the level of correlation is rather sufficient for the majority of the stations. Low degree of correlation coefficients, below 0.5, is displayed for eight stations alone. These discrepancies can be attributed to spatiotemporal shifts of modeled versus observed rainfall patterns as well as sub-grid scale phenomena.

A spatial examination of the modeled precipitation estimates is provided in Figure 4, illustrating the MBE, MAE, RMSE and correlation results in the locations of the stations under consideration. Cumulatively, lower errors can be traced in the North mainland of the Peninsula and greater in the stations distributed in the West and Southwest. This is mainly due to the higher precipitation amounts in these regions. It could be also attributed to the terrain elevation changes, increasing from the shoreline to the mainland. These topographical characteristics together with the offshore convective activity increase the uncertainty in the spatial and temporal estimation of rainfall.

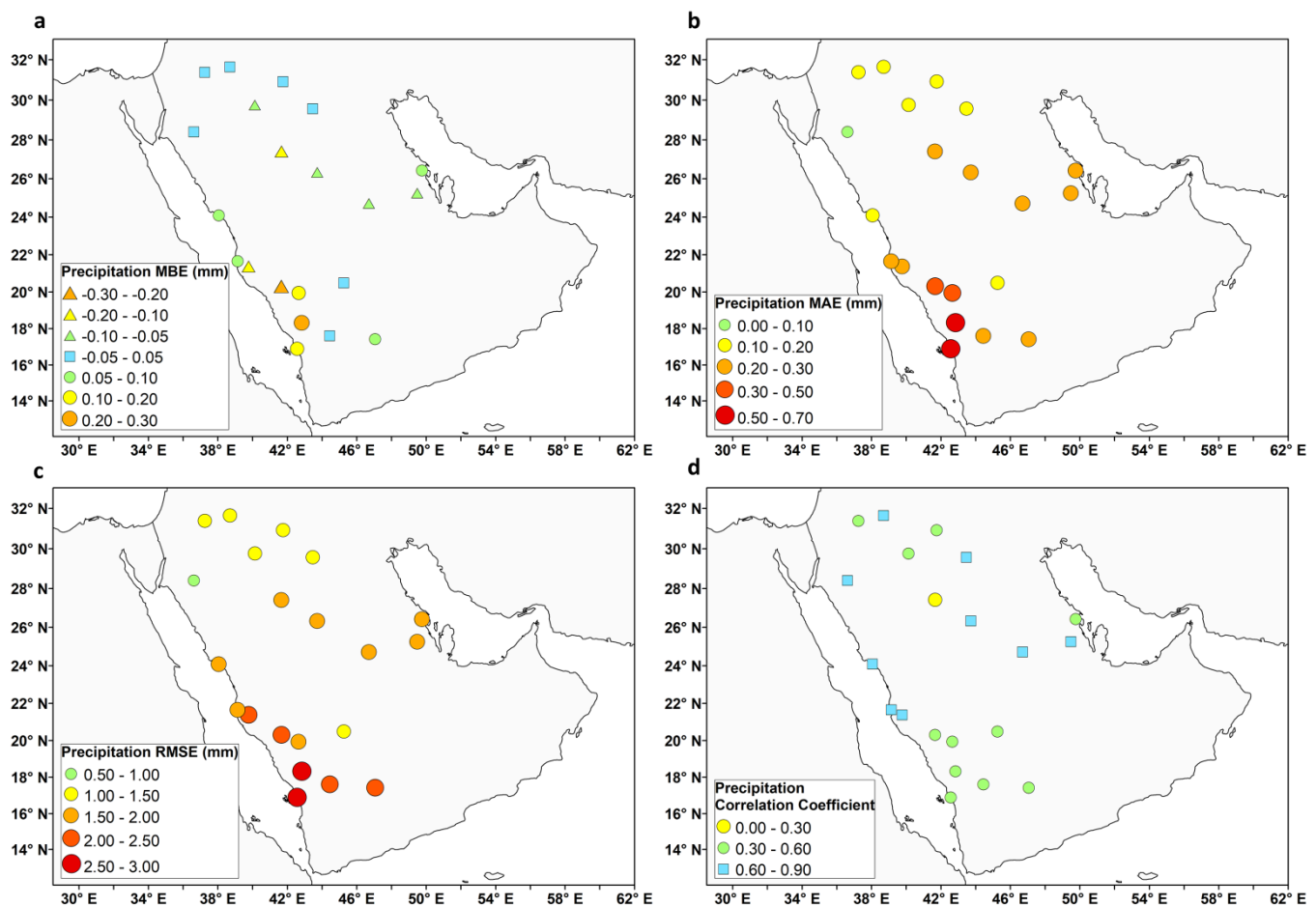


Figure 4. (a) MBE, (b) MAE, (c) RMSE and (d) Correlation Coefficient between modeled and station precipitation data.

To further assess the performance of the simulated precipitation fields, an evaluation analysis for each year was performed. This is presented through the creation of weighting error plots for the MBE and MAE statistical indicators across the whole examination period (Figure 5). The range of inter-quantiles bounds and maximum/minimum values around the MBE and MAE medians is considerable due to the extent of the domain under study that encloses areas with diverse meteorological characteristics. Systematic errors, provided via the MBE, are centered close to 0 mm, with a small variation of approximately ± 0.1 mm. Larger deviations per year are present in the median MAE values with values remaining below 0.25 mm in most of the years.

Relevant weighting error plots have been constructed for an inter-annual evaluation analysis (Figure 6). Most of the MBE values are close to zero, with a small underestimation found in January. Error ranges are wider from January to April and from October to December. Similar results are also evident for the MAE values, with the largest errors presented in April. This is rather expected, considering that within these months, precipitation is more frequent and with higher rates, leading to spatial and temporal discrepancies.

In order to understand the precipitation features and the climatic characteristics affecting them, the following chapters focus on: (i) a mean annual and monthly accumulated precipitation analysis to assess the seasonal changes in rainfall patterns, (ii) a trend analysis investigating the changes in the precipitation amount through this 30-year period and (iii) an intensity–duration–frequency analysis focusing on precipitation events that cause floods every year.

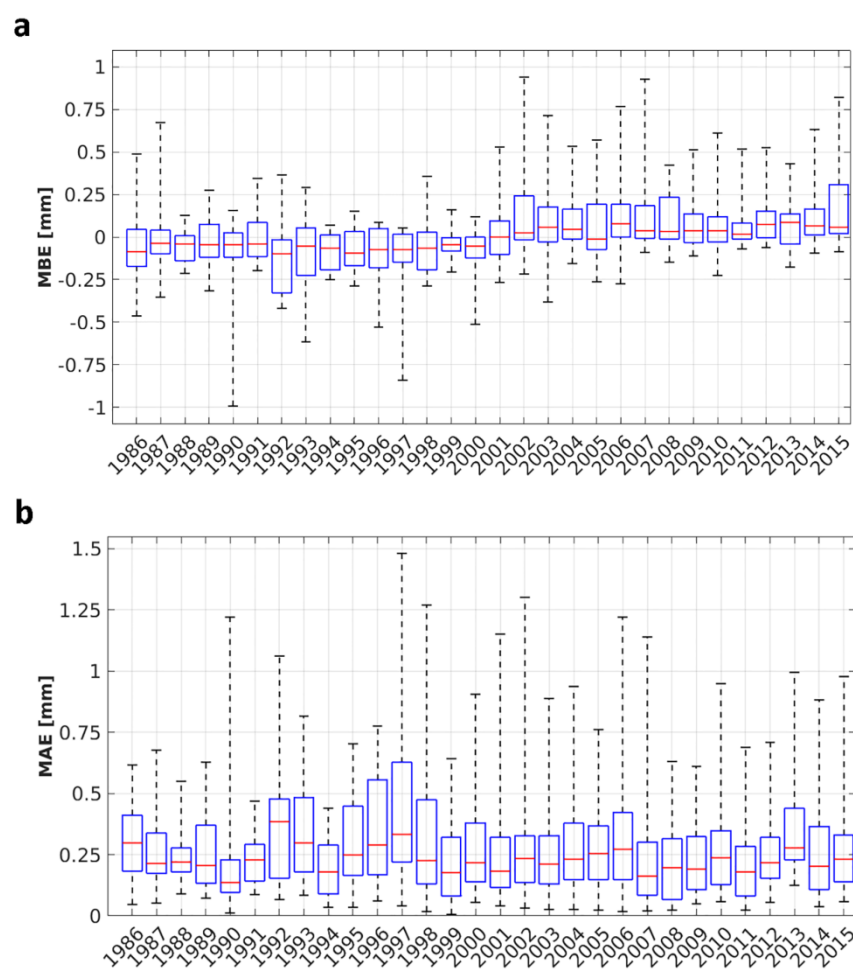


Figure 5. (a) MBE and (b) MAE annual variation between modeled and station precipitation data. Central red marks display the median, box edges display the range between the 25th and 75th percentiles and the whiskers point to the minimum and the maximum values, respectively.

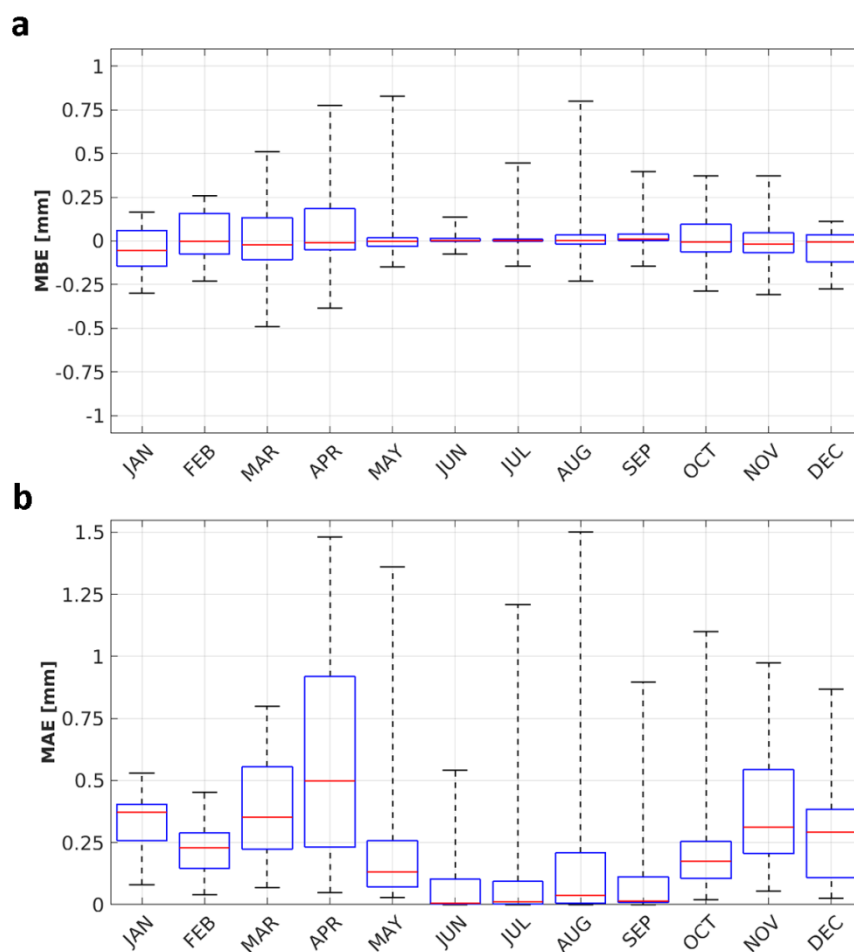


Figure 6. Inter-annual (a) MBE and (b) MAE variation between modeled and station precipitation data. Central red marks display the median, box edges display the range between the 25th and 75th percentiles and the whiskers point to the minimum and the maximum values, respectively.

3.2. Mean Annual and Monthly Accumulated Precipitation

Rainfall in AP is mostly an outcome of convection processes. There are intense local-scale events that often lead to floods. The duration of precipitation is short, typically lasting for a few hours. This highly localized nature and the short duration of precipitation makes its monitoring a challenging procedure. On an annual basis, the mean accumulated precipitation distribution (Figure 7) reveals that the southwest region of the AP receives the highest amount of precipitation throughout the whole year due to the orographic enhancement of precipitation and the increased convective activity. On the contrary, there are two dry regions: the northwestern region (an extension of the Egyptian dry zone) and the southeastern region, over the Rub Al-Khali, the world's largest sand desert.

Precipitation mostly occurs from October to April (Figure 8). During winter, rainfall is mainly an outcome of the Mediterranean cyclones and frontal zones. Secondary low-pressure systems that develop under favorable upper-level conditions, involving upper-level troughs and jet interaction may also contribute. Furthermore, cold air advection from the northeast, due to the extension of the Siberian high, meets the warm humid air coming from Sudan over the southern Red Sea through a corresponding trough (Figure 9a). The latter tends to cause rainfall due to both instability and orography [41]. There are cases when weather systems move southward along the Red Sea trough and provide winter precipitation as far south as Mecca and sometimes as far as Yemen. In March and April, limited precipitation, often torrential, occurs. In summer, the highlands of Asir receive

great amounts of rainfall affected by the monsoonal winds to support a steppe-like strip of land.

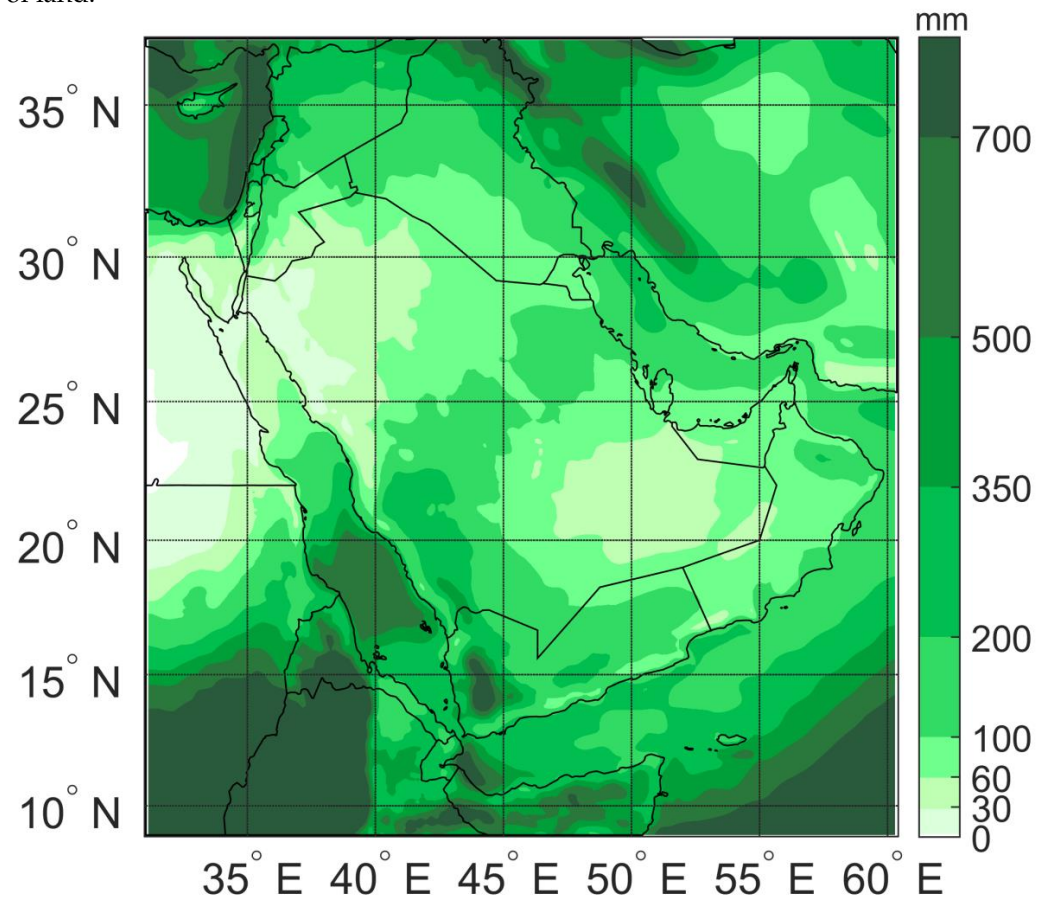


Figure 7. Mean annual accumulated precipitation for the years 1986–2015 (model output).

During March, the desert front that forms during the transitional period of spring across southern Egypt and the northern Red Sea into central Saudi Arabia results in the formation of a secondary wave over the central Red Sea (Figure 9b) associated with extensive thunderstorms and intense precipitation. In April, thunderstorms and heavy rain are associated with convective activity due to the passage of desert fronts and the thermal trough of Sudan.

In summer, the Mediterranean systems do not affect the region. The monsoon southwesterlies that affect the peninsula (Figure 9c) are conditionally unstable and provide moisture; therefore, they can induce thunderstorms, mainly in the southwestern part. October and November are the months when the rainfall is associated with secondary lows, generated in the examined region or Mediterranean, depressions and fronts that move towards the central AP (Figure 9d).

The southwestern part of the Arabian Peninsula is characterized by mild steppe climate in contrast to elsewhere, where a hot desert climate is met. This is attributed to the fact that rainfall is relatively frequent, especially during winter and spring. The precipitation climate of this part is influenced by the Red Sea, the topography of Arabian Peninsula and Eastern Africa and the Indian Ocean monsoon [41].

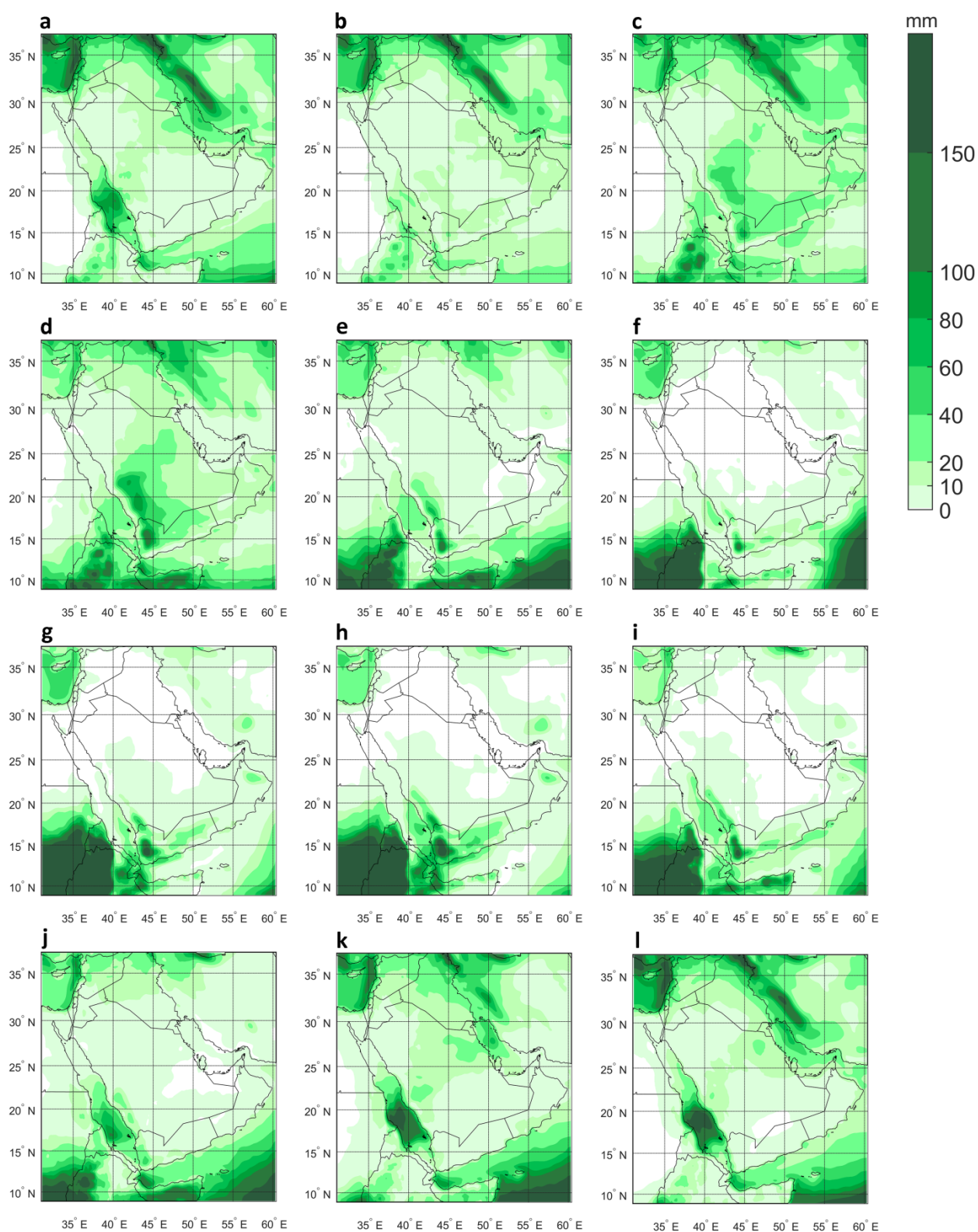


Figure 8. Mean monthly accumulated precipitation (modeled) for (a) January, (b) February, (c) March, (d) April, (e) May, (f) June, (g) July, (h) August, (i) September, (j) October, (k) November and (l) December.

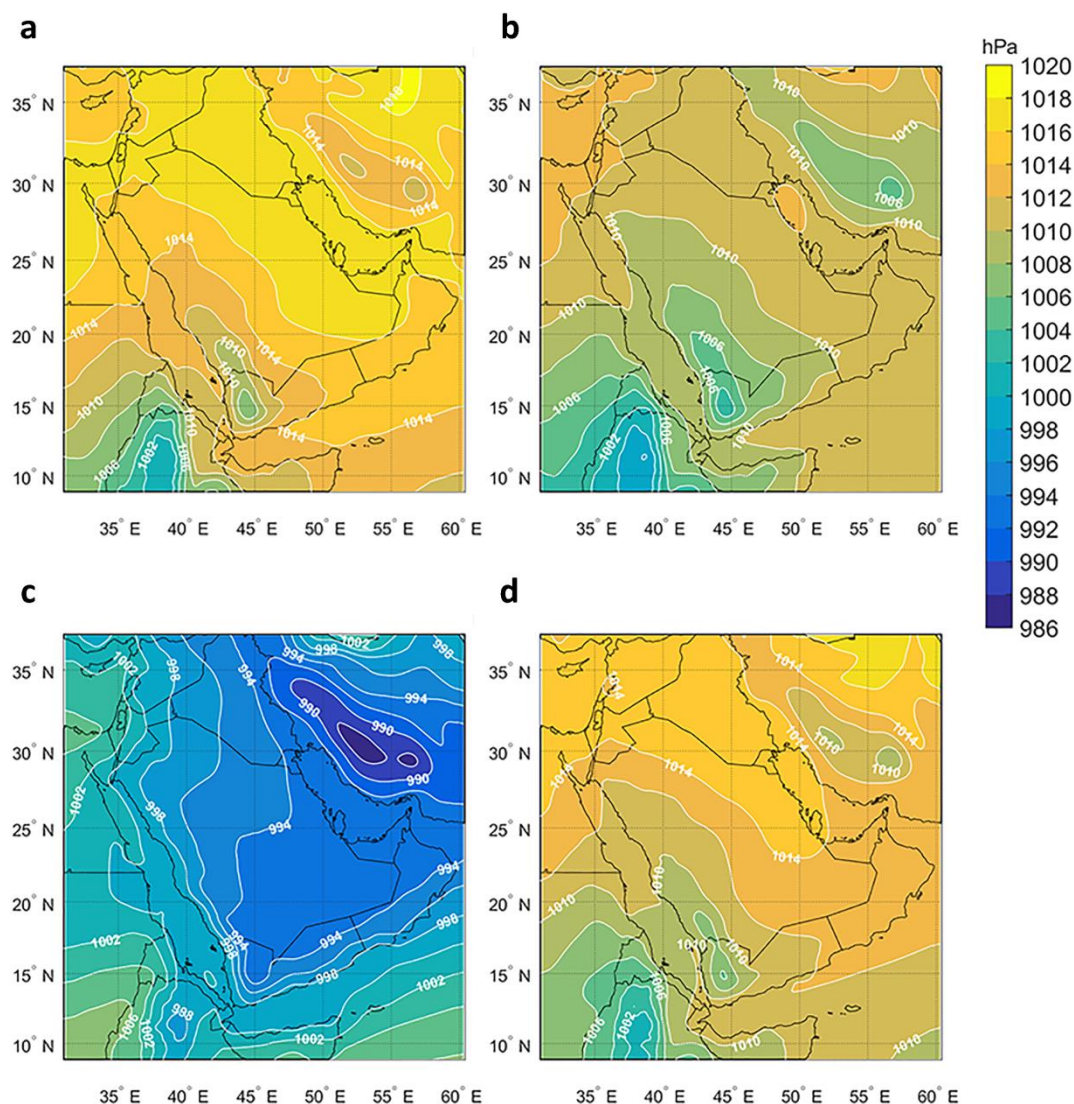


Figure 9. Mean monthly values of Sea Level Pressure for (a) January, (b) March, (c) July and (d) November.

3.3. Trend Analysis

The number of studies focusing on the estimation of rainfall trends in the AP employing either observational or modeled datasets is rather limited [1,4,42,43]. Therefore, the spatiotemporal density and the extent of this database can be an added value in understanding the recent changes in the precipitation patterns and behavior. To this end, the implementation of both monthly and annual approaches was decided for this study. The calculated trends are based on the nonparametric approach by Sen (1968). The depicted output was found to be statistical significant, tested at a 0.05 significance level using the Mann–Kendall’s test [44,45]. For the sake of simplicity, the results were integrated to a ten-year period and normalized by the accumulated precipitation of the same reference period.

The spatial distribution of the accumulated precipitation trends on an annual basis presents insignificant percentage values in the time period 1986–2015 (Figure 10). There is, however, a decrease of about 0.5% per decade observed over the eastern part of the Empty Quarter. Even if this magnitude appears to be trivial, it is essential as it affects a large sand desert located in the southern borders of Saudi Arabia, including also parts of Oman, United Arab Emirates and Yemen. This comes in general agreement with previous studies that investigate changes in precipitation observations in AP.

Hasanean and Almazroui [1] resulted in an estimated reduction in rainfall over the Arabian Peninsula for the period 1978–2009. Contrary to what it is observed here, the annual precipitation decreased over northern regions of the Peninsula and increased over the south. The estimation, however, was performed employing datasets with a 10-year shift as compared to the dataset used here. At the same time, Almazroui et al. [4] found insignificant changes during the period 1979–1993 and a decrease over the period 1994–2009. Moreover, AlSarmi and Washington [5] reported an insignificant but yet a negative trend in precipitation in a study covering the time period 1986–2008.

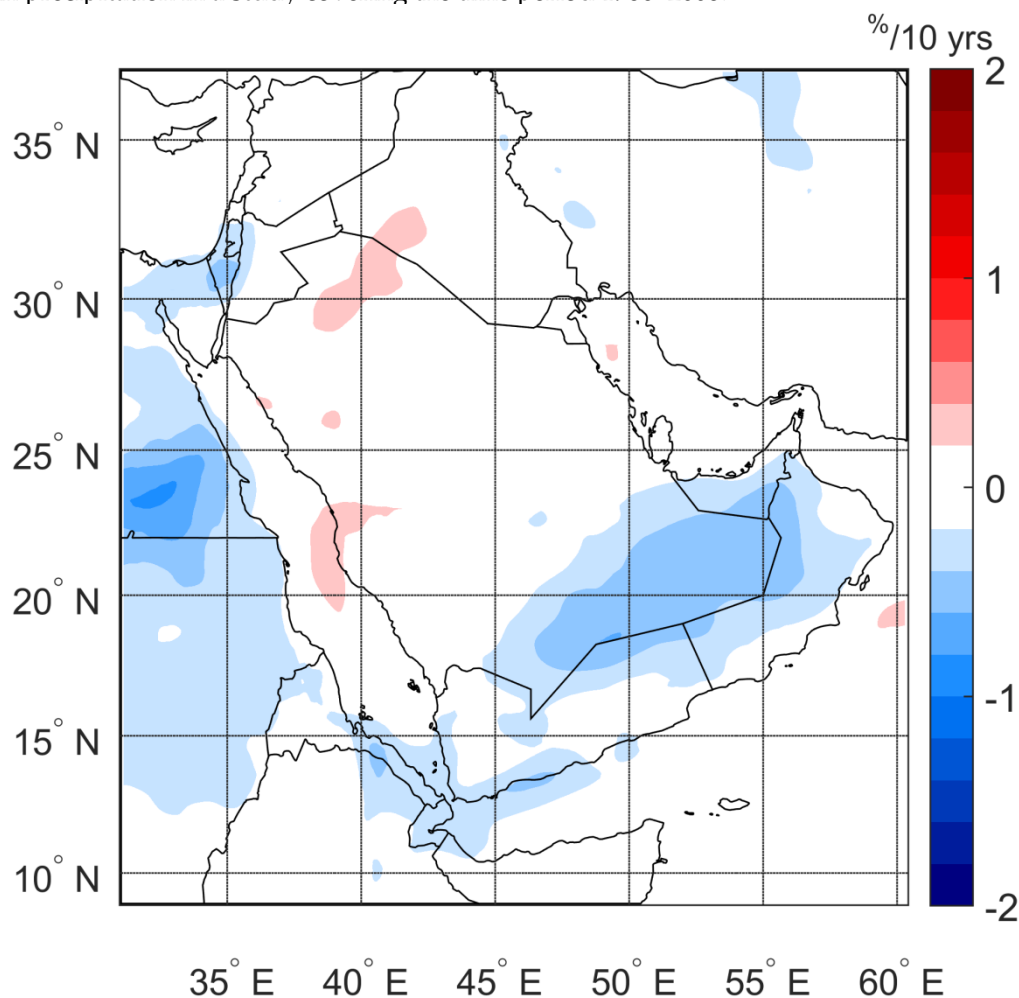


Figure 10. Annual accumulated precipitation (modeled) change (percentage) per 10 years.

Despite the fact that the inter-annual changes of the accumulated precipitation were found to be insignificant, the monthly changes are quite interesting (Figure 11). There are both positive and negative trends depending on the month under investigation with a range of approximately 2% around zero. However, it should be mentioned that each percentage change should be studied alongside (and compared to) the mean monthly accumulated precipitation discussed earlier. The reason behind this suggestion is that sometimes considerable percentage changes refer to small amounts of precipitation, rendering them rather insignificant from a practical point of view.

A general remark would be that there is a seasonal shift on the accumulated precipitation as neutral to negative trends, observed from December to April and rather positive trends over the remaining months. In December, a decrease of about 5 mm/decade is visible in mid-North Peninsula. A slightly lower decrease is found in January accompanied with a positive trend of about 5 mm/decade in the north of Medina. Larger deviations with a decrease of more than 10–15 mm/decade emerged from February to April alongside the borders of Saudi Arabia, Oman and Yemen with the highest values to be traced over

the northern parts of Yemen during April. A small increase in the order of 5–10 mm per decade (maximum) is the case regarding the rest of the months. The large changes found over sea are a result of the normalization process. They could be also linked to reasons like model bias and SST anomaly. Therefore, no special focus is dedicated as the information could be misleading. It is evident that the trends on an annual basis (Figure 10) are mostly dominated by the winter/wet season changes (Oct–Apr, Figure 11). As stated earlier, the large percentage changes found during the dry season may result in small actual rainfall changes and a negligible impact.

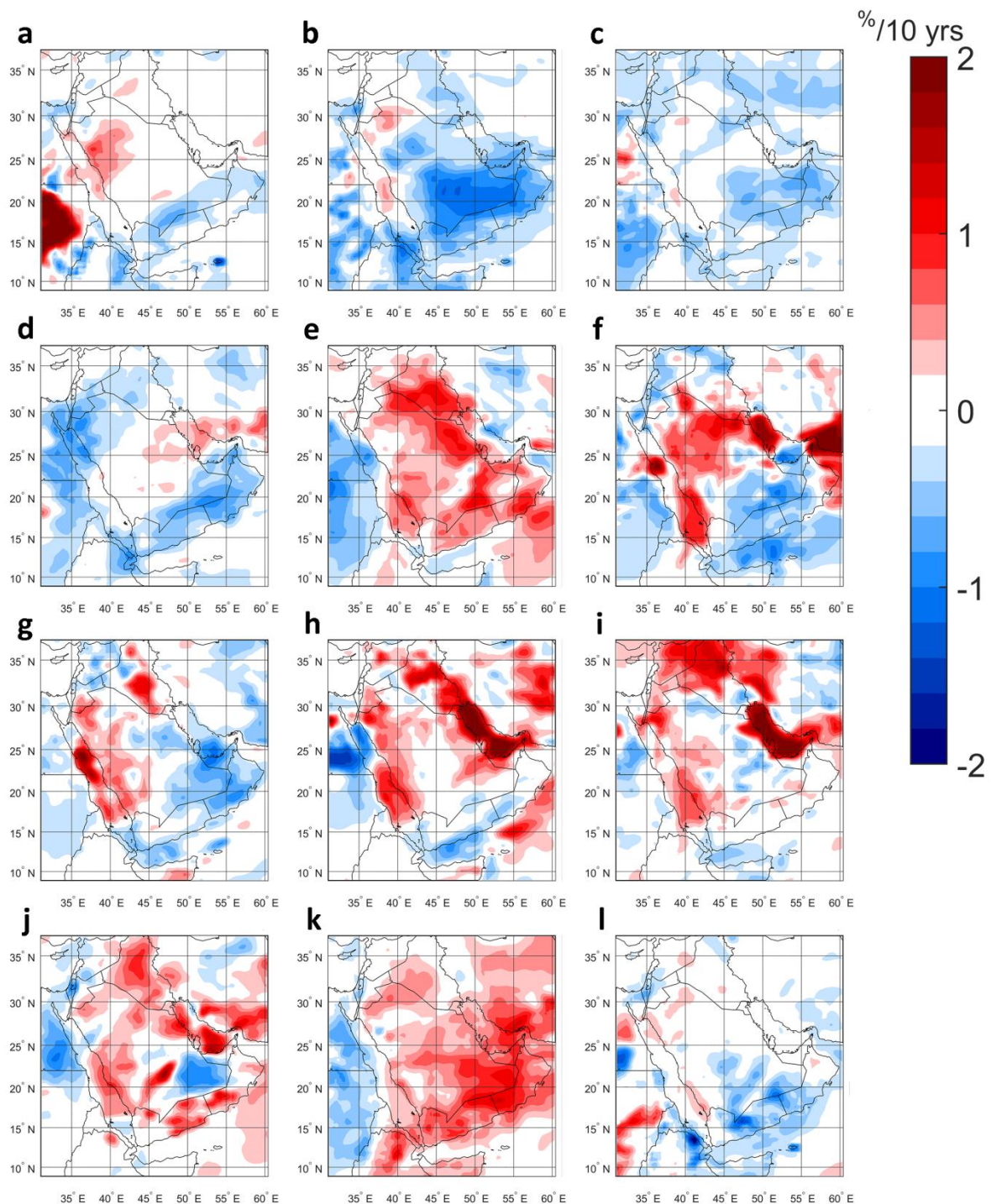


Figure 11. Monthly accumulated precipitation (modeled) change per 10 years for (a) January, (b) February, (c) March, (d) April, (e) May, (f) June, (g) July, (h) August, (i) September, (j) October, (k) November and (l) December.

Precipitation is an important factor for various activities in the region due to its scarcity. However, floods and/or flash floods tend to cause extensive problems on infrastructure and pose threat to human life as they often lead to casualties. In many cases, extreme rain rates associated with thermal convection are observed. During such intense rainfall events, runoff flows from the hills and mountains towards lower heights, causing flash floods in urban areas. This is also associated with the dryness of the soil and the absence of dense vegetation. Therefore, the study of the intensity and the duration of extreme precipitation events is more than valuable to a variety of sectors from engineers to civil protection agencies.

3.4. Extreme Value Analysis (Intensity, Duration and Frequency)

The intensity related to the duration and probability of occurrence of rainfall events can provide useful information regarding the potential impact of extreme cases. Therefore, an analysis has been performed for specific locations. The sites (Figure 1) were selected due to their importance based on population, economic and cultural characteristics and in order to be representative of the region's various climatic patterns.

Beginning with the locations in the eastern part of the AP, the average rainfall intensity for different durations and return periods, appears to be similar in terms of magnitude (Figure 12). A 3 h event with average rain rate of 4–5 mm/h is expected in Kuwait city, Buraydah, Manama, Doha, Dubai, Abu Dhabi, Muscat and Salalah every 8–10 years. Extreme events over these areas are rather convective with duration in the scale of minutes to an hour. Events with longer return periods could affect the same areas with 21–24 mm accumulated precipitation over 3-h duration and an average rain rate gradually falling for larger durations. Around 50 mm is expected over a 12-h period and a 1% probability of occurrence. Slightly higher rates are found in Riyadh with the 3-h accumulated precipitation ranging between 20 and 35 mm for a 10- and a 100-year return period, respectively. A quick reduction in rainfall intensity is observed in larger durations, resulting in similar patterns, as in the rest of the locations. This is rather expected due to the nature of the atmospheric systems.

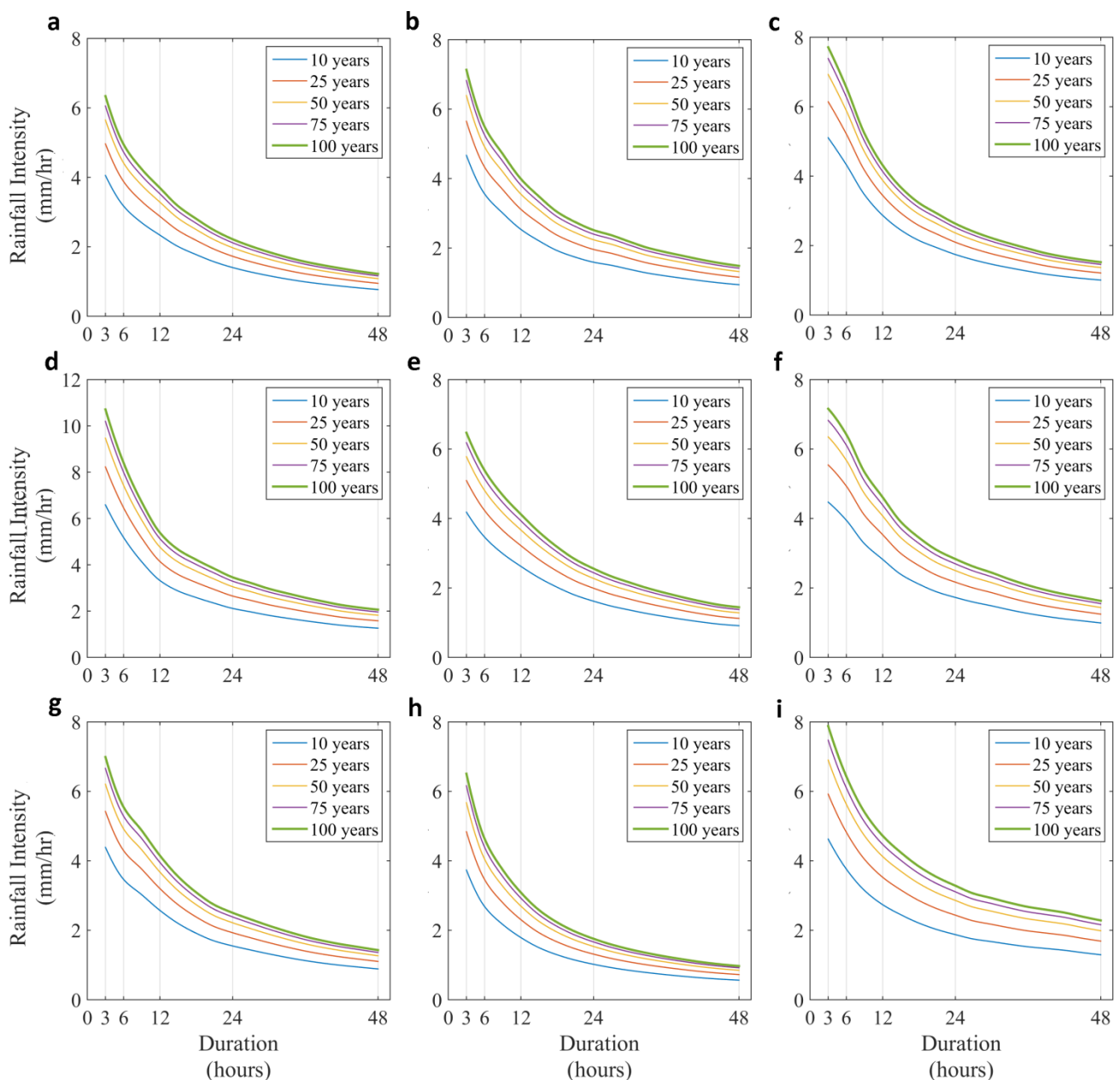


Figure 12. IDF curves (modeled output) for selected locations/cities in the east part of the Arabian Peninsula: (a) Kuwait city, (b) Burayadah, (c) Manama, (d) Riyadh, (e) Doha, (f) Dubai, (g) Abu Dhabi, (h) Muscat and (i) Salalah.

The western part of the AP is characterized by a greater variability (Figure 13). It is highly affected by the Mediterranean lows in the north and the monsoonal activity in the south. An additional characteristic is that the humidity of the air masses affecting this part is higher due to the presence of neighboring warm seas, such as the Mediterranean Basin in the north, the Red Sea in the east and the Sea of Aden in the south. Therefore, heavier precipitation events are generally expected. However, this is not evident in all locations as different rainfall patterns are observed. Beginning with the more arid areas, Arar, Tabuk, Hail and Medina are characterized by lower values compared to the eastern side. Precipitation is rare and extreme events are less likely to take place. Jeddah, Mecca and Jazan have quite comparable behavior. This can be attributed to their similar climatic characteristics. They are all nearshore locations, affected by the warm and humid air masses originating from the Red Sea. The existence of Azir and Sarawat mountains on the east of the aforementioned cities often causes orographic lifting of the wind flow

leading to convection and extreme precipitation events. A total of 30 mm of accumulated precipitation over a period of 3 h can be expected in Jeddah and even higher values in Mecca and Jazan. However, the rain rate is quickly reduced in longer durations, especially in Mecca, something that further highlights the short duration of precipitation over the region. Sanaa on the other hand is characterized by a wet climate. It is located in an altitude of 2250 m receiving more than 200 mm/year (Figures 2 and 7). Extreme events with a rainfall intensity of more than 22 mm/h and duration of about 3 h are expected at a 10-year frequency. Although extreme events are more likely to happen in this particular region, they have the same characteristic when it comes to their duration. Therefore, for a 10-year recurrence interval, around 65 mm of accumulated precipitation is expected within a period of 3 h and 130 mm within 12 h. This means that quadrupling the duration leads to a doubling of the total amount of precipitation. Aden is a sea side location characterized by increased humidity [10] with low amounts of precipitation, yet higher than most of the other locations examined.

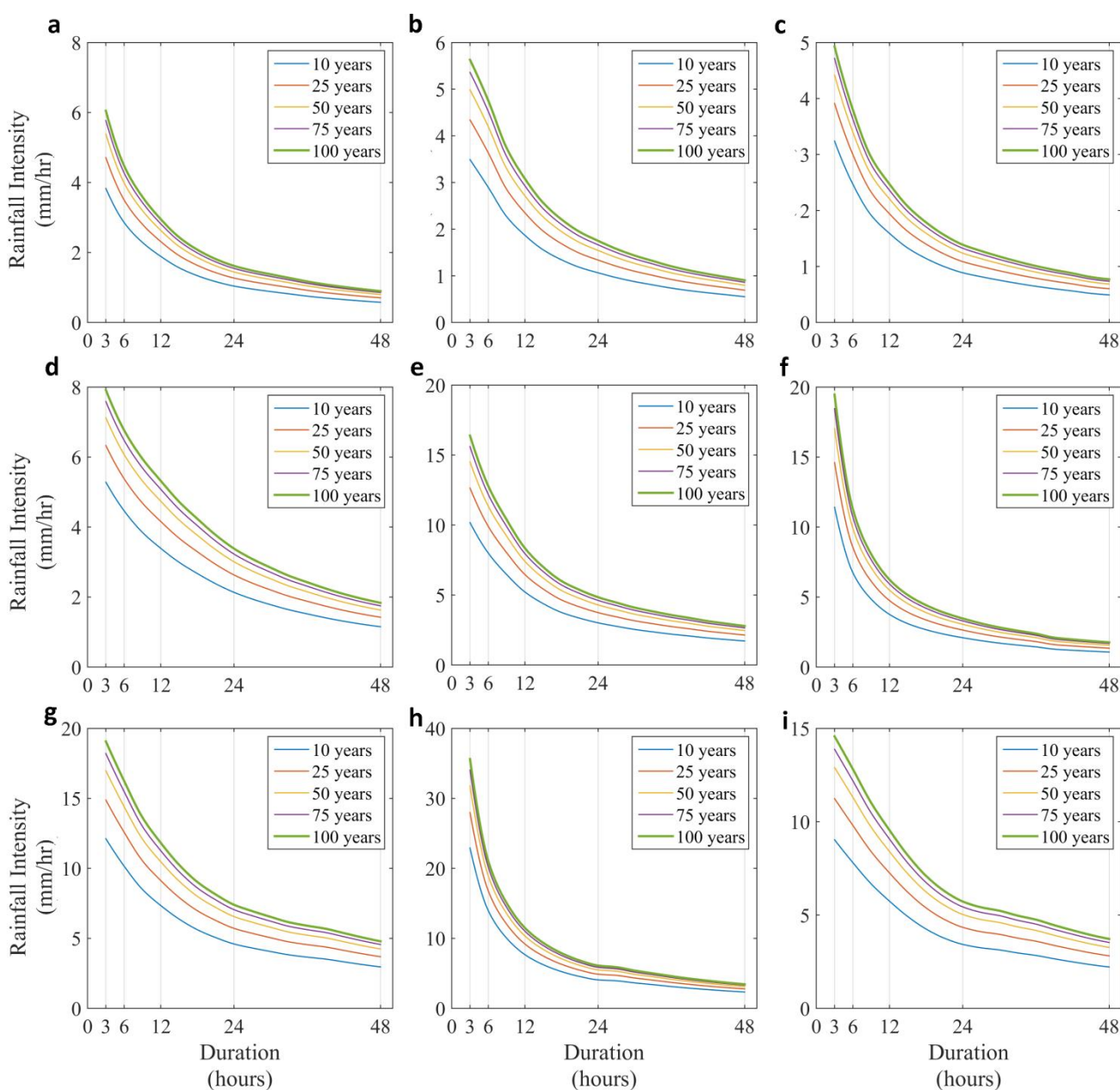


Figure 13. IDF curves (modeled output) for selected locations/cities in the west part of the Arabian Peninsula: (a) Arar, (b) Tabuk, (c) Hail, (d) Medina, (e) Jeddah, (f) Mecca, (g) Jazan, (h) Sanaa and (i) Aden.

A better understanding of the behavior of extremes in the region requires the examination of the spatial distribution of the relation between the intensity, the duration and the frequency of precipitation events. However, it is practically impossible to depict 3D information over a printed map. Therefore, in order to be able to have an overview of this behavior, the average intensity of a hypothetical event for selected durations and return periods was estimated. More specifically durations equal to 3, 6, 12 and 24 hours and return periods equal to 25, 50 and 100 years were selected (Figure 14, Figures A2 and A3).

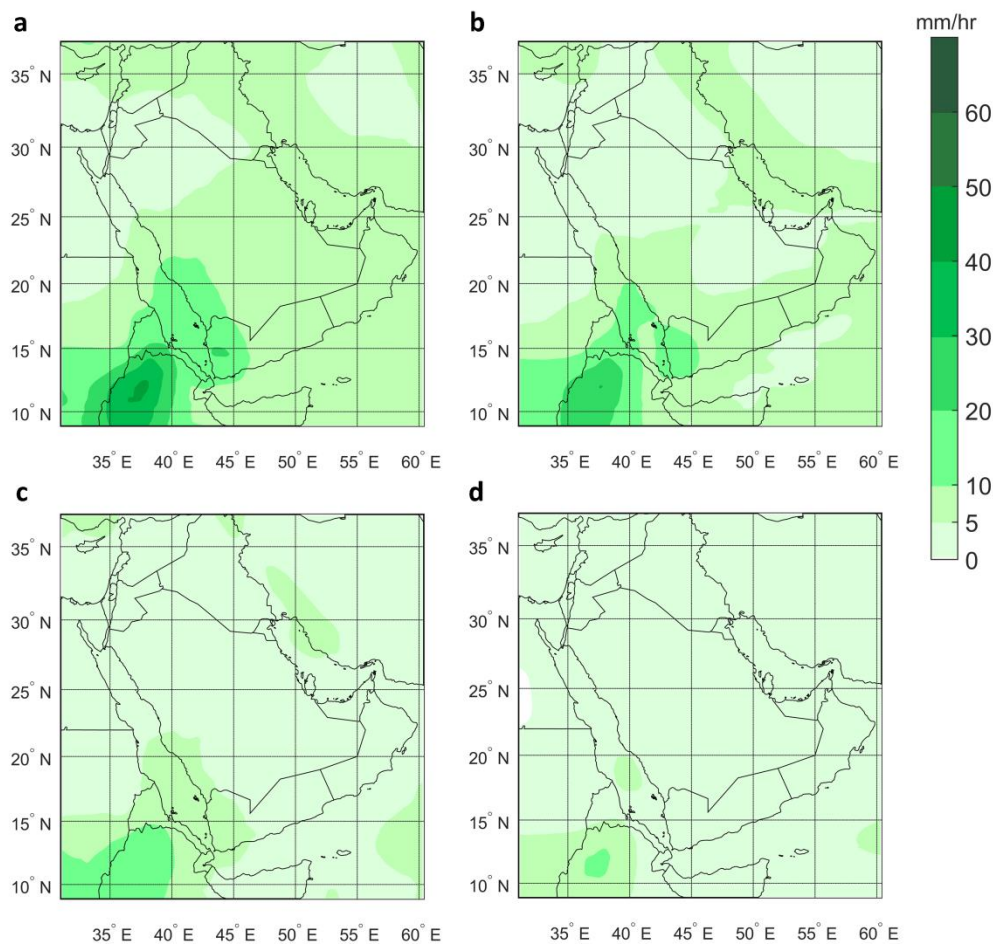


Figure 14. Average rainfall intensity (modeled) for durations of 3, 6, 12 and 24 hours (a–d, respectively) and a 25-year return period.

The general pattern of the spatial distributions regarding the average rainfall intensity for all durations and return periods follows that of the mean annual accumulated precipitation (Figure 7). As expected, the precipitation rate drastically falls for larger durations. In particular, for durations greater than 12 hours, it is practically an artificial outcome of the averaging taking place during the application of the extreme value methodology described earlier, with an exception of the areas located southeast. This bottom half-coastal region in the east is the most affected by extreme events, something already expected from the discussion on the intensity, duration and frequency relations in Mecca, Jeddah, Jazan and Sanaa. This zone receives precipitation with intensities between 10–20 mm/h and an average duration around 3 h once every 25 years. Slightly lower values but with a same pattern are observed for 6-h events. At higher return periods, intensification is expected. However, an “upper bound” is observed as maximum values tend to converge.

4. Conclusions

The Arabian Peninsula is one of the most important economic regions in the world and home to more than 80 million people. Its prevailing climatic characteristics belong to the desert climate in the Köppen classification, with high temperatures, low rainfall and strong dust presence. This leads to low levels of soil moisture and water supply, affecting agriculture and human activities in general. At the same time, intense precipitation events cause floods every year with severe damages and casualties. Therefore, an extensive analysis of the climatic precipitation features deemed necessary. The limited amount of in situ observations over large parts of the peninsula was a restrictive aspect in terms of a climate oriented analysis. In this study, this was confronted through the employment of a state-of-the-art atmospheric model. The model was used for the regional analysis covering the entire peninsula and provided atmospheric data for 30 years with a temporal resolution of 9 km and a spatial resolution of 3 hours. The atmospheric model performance in the representation of the rainfall patterns was thoroughly examined through a qualitative and quantitative analysis. In situ and satellite data were deployed and their juxtaposition with model outputs was indicative of a reliable model behavior. The mean accumulated precipitation spatial distribution and variations were efficiently captured both on an annual and a monthly basis. The output efficiency was also supported by the good statistical indices.

The analysis was performed in three main components; the mean climatic characteristics, the rainfall trends and the extreme cases. Beginning with the spatial distribution of the mean annual accumulated precipitation, higher accumulation values were evident in the southwest due to the topographic characteristics. On the contrary, two dry regions emerge, the northwestern one as an extension of the Egyptian dry zone and the southeastern one over the Rub Al-Khali, the world's largest sand desert. In the monthly analysis, lower precipitation was generally evident from October to April. During winter, rainfall was associated to the passage of low pressure systems originating from the Mediterranean Sea and the cold air being advected from the northeast. In the second scenario, air masses met the warm humid air over the southern Red Sea causing rainfall. In March and April, intense convective activity and heavy rain events might occur. During summer, the region is not affected by the Mediterranean systems. The monsoon southwesterlies often cause thunderstorms mainly in the southwestern part of the peninsula. Rainfall in October and November is associated with secondary lows generated over the Mediterranean.

Another important issue to address when investigating the climatic characteristics of precipitation over a particular region is the potential changes on the total rainfall amount received. The spatial distribution of the accumulated precipitation trends revealed insignificant percentage differences in the time period of interest. A slight decrease, however, was observed over an extensive area covering the largest desert of the peninsula, across the Saudi Arabian borders. Regarding the monthly analysis, a seasonal shift on the accumulated precipitation was evident. Neutral to negative trends were observed from December to April and positive in the remaining months.

In most cases, precipitation in the region occurs as an outcome of convection. It has a highly localized nature and a tendency to cause floods despite its short duration. The behavior of intense precipitation was examined through an extreme value analysis. The analysis took into consideration the intensity and the duration of a precipitation event simultaneously. The eastern parts of the peninsula presented the lowest risk associated with extreme events. Slightly higher rates, however, were met in Riyadh. The pattern in the western domain was more interesting. The top half experienced a similar pattern with the East. This was not the case, however, in the southwest, where a coastal zone affected by the warm Red Sea and the Sea of Aden, the mountains of Azir and Sarawat and the monsoonal activity faced the highest risk. Over this area, events with 3-h accumulated precipitation values over 50–60 mm were quite frequent in terms of return periods. These values were even higher in higher elevations.

The precipitation patterns and their variability often pose a global socioeconomic threat, let alone affecting the local population. This paper is an effort to outline the detailed climatic characteristics of precipitation in the Arabian Peninsula in space and time, which is especially important in a climate-changing environment. The outcome has an added value in terms of civil protection and industry applications such as constructions and reinsurance. However, a further examination of the behavior of additional contributing parameters will follow. This will provide a more sophisticated insight and a deeper understanding of the processes and their expected impact in the forthcoming years.

Author Contributions: Conceptualization, P.P., H.F. and G.K.; methodology, P.P.; software, P.P.; validation, C.S.; formal analysis, P.P.; investigation, P.P.; resources, G.K.; data curation, P.P.; writing—original draft preparation, P.P., H.F. and C.S.; writing—review and editing, N.S.B.; visualization, P.P.; supervision, G.K.; project administration, G.K.; funding acquisition, G.K. All authors have read and agreed to the published version of the manuscript.

Funding: This work was supported by Saudi Aramco, Contract No: 6600033903 to WeMET P.C.

Data Availability Statement: The data presented in this study is available on request from the corresponding author.

Acknowledgments: We would like to acknowledge the National Center for Meteorology of Saudi Arabia and Mohammed Ahmed Alomari in particular, for the rain gauge data provided. Special thanks to the Saudi Aramco Employees Jumaan Al Qahtani, Ioannis Alexiou, Ayman for their fruitful collaboration. Nikolaos S. Bartsotas current affiliation is the National Observatory of Athens, Institute for Astronomy and Astrophysics, Space Applications and Remote Sensing—BEYOND Center of Earth Observation Research and Satellite Remote Sensing, Athens, Greece.

Conflicts of Interest: The authors declare no conflict of interest. The funders had no role in the design of the study; in the collection, analyses, or interpretation of data; in the writing of the manuscript, or in the decision to publish the results.

Appendix A

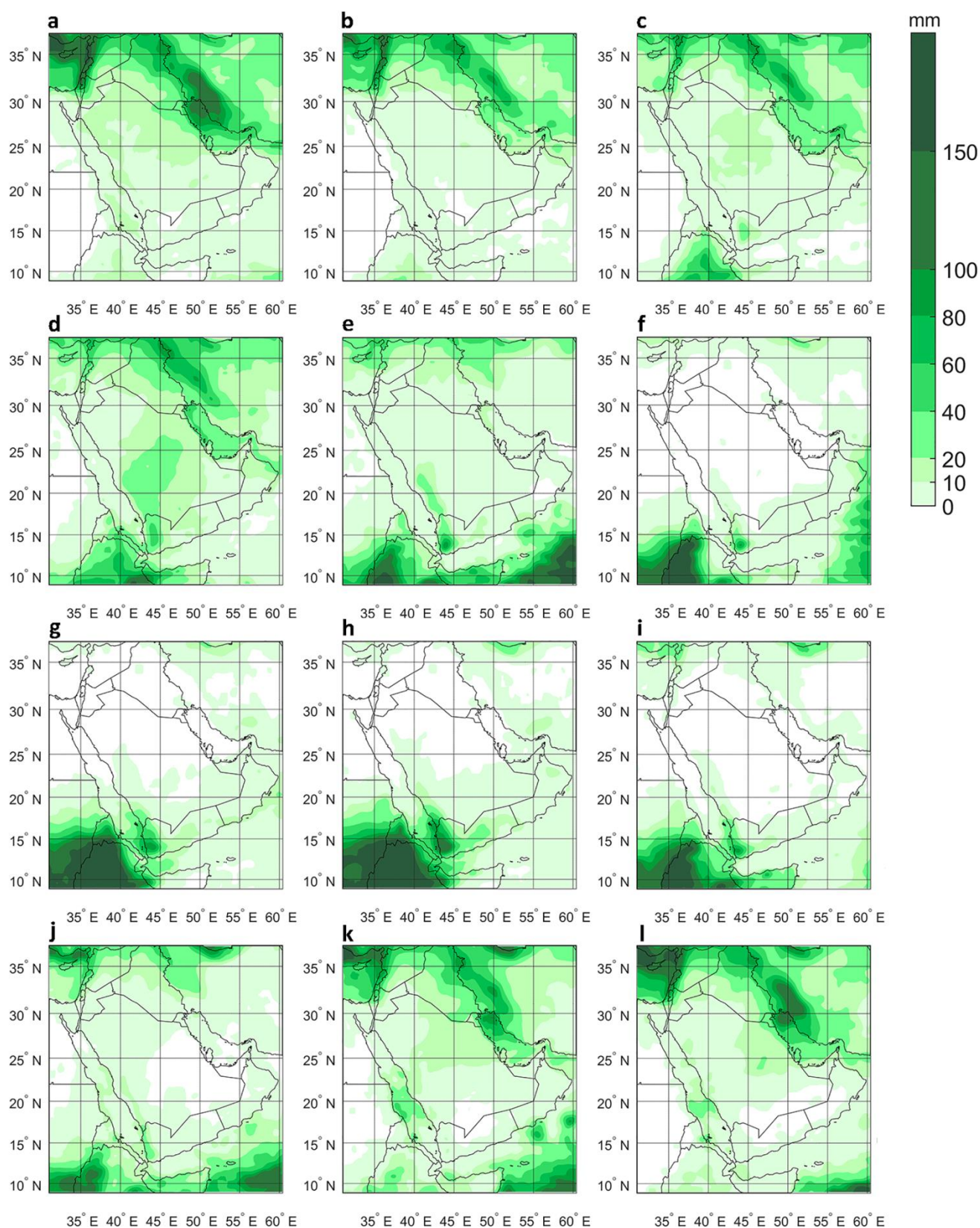


Figure A1. Mean monthly accumulated precipitation (IMERG) for (a) January, (b) February, (c) March, (d) April, (e) May, (f) June, (g) July, (h) August, (i) September, (j) October, (k) November and (l) December.

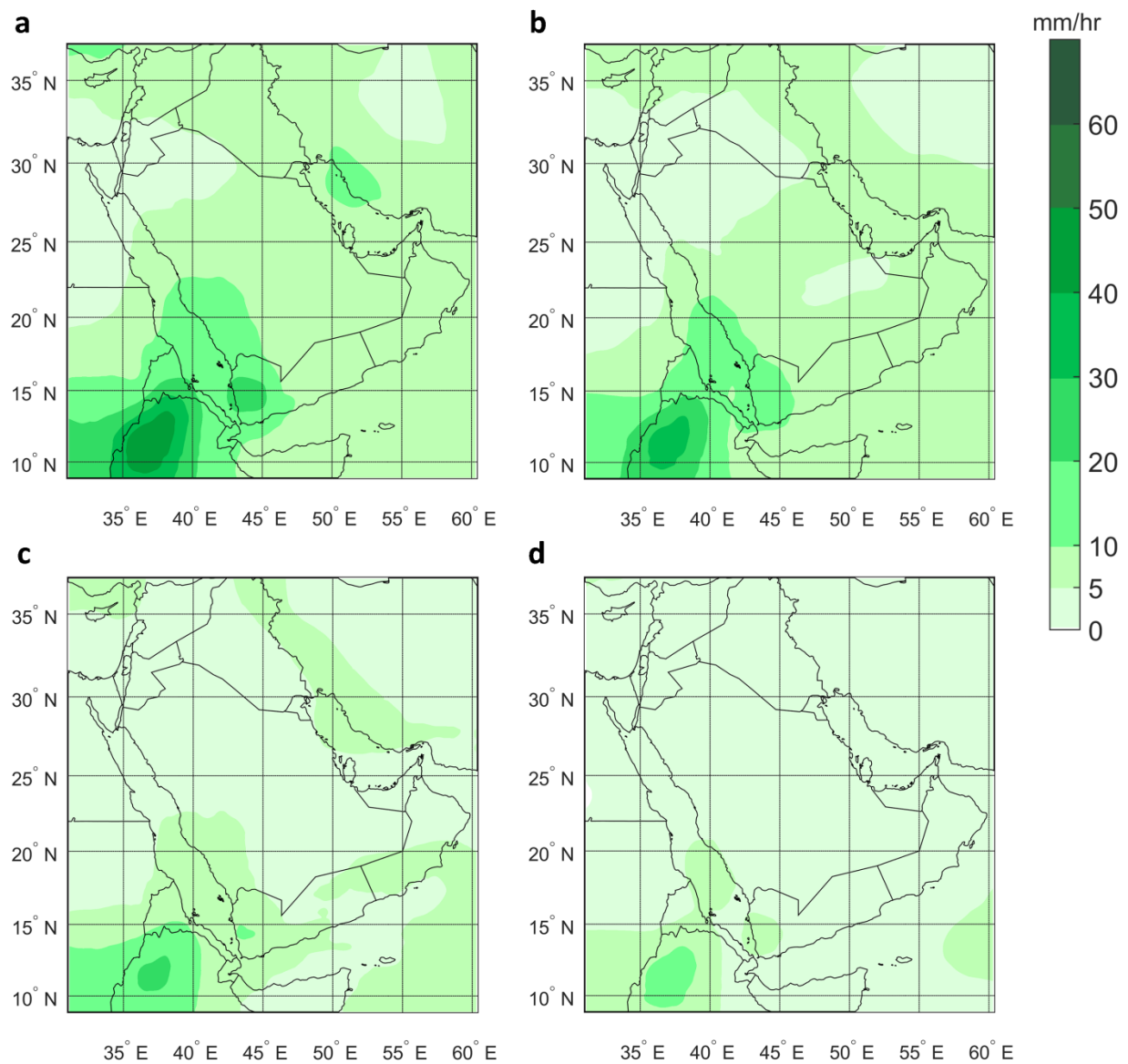


Figure A2. Average rainfall intensity (modeled) for durations of 3, 6, 12 and 24 hours (a–d, respectively) and a 50-year return period.

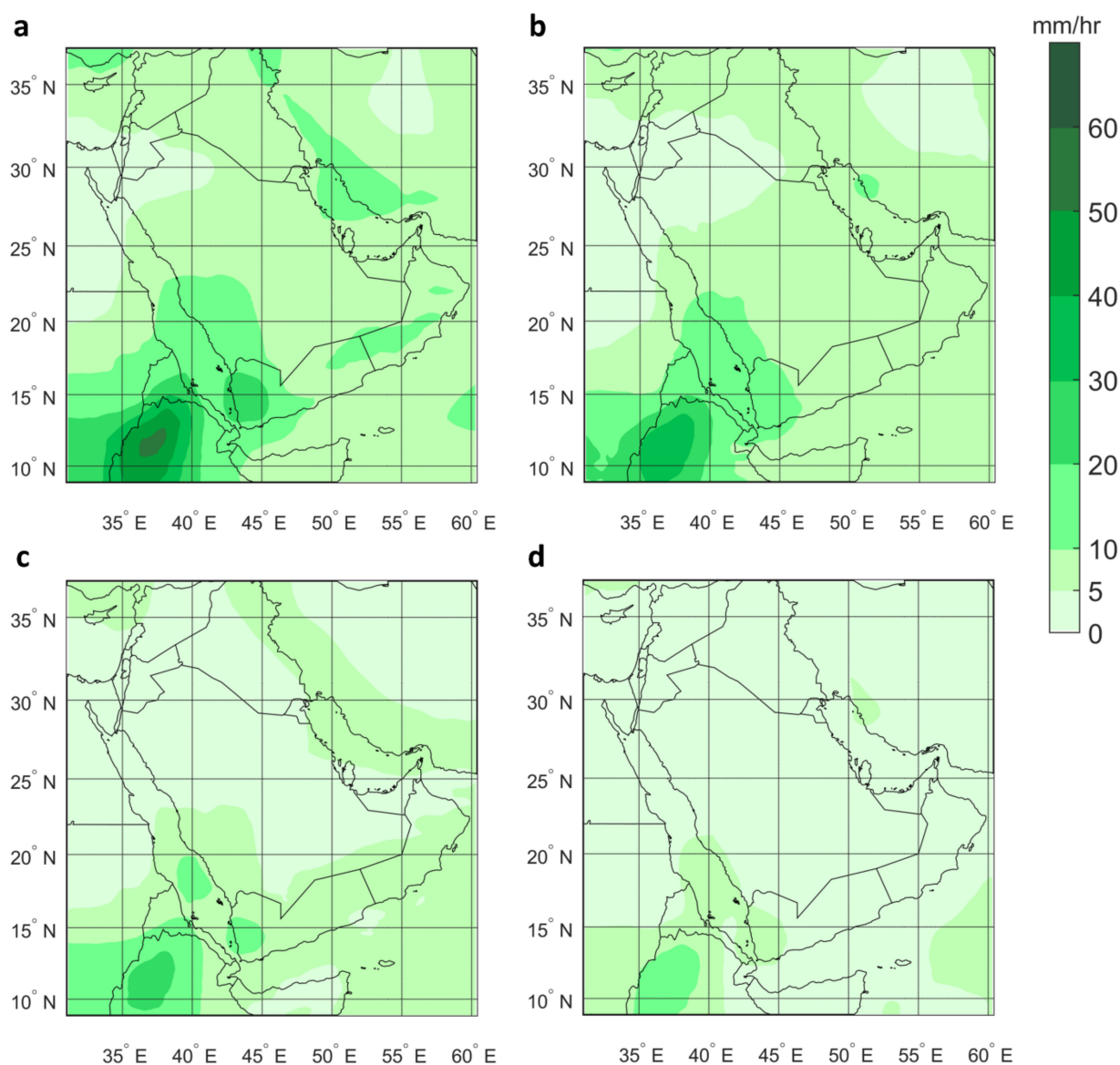


Figure A3. Average rainfall intensity (modeled) for durations of 3, 6, 12 and 24 hours (a–d, respectively) and a 100-year return period.

References

1. Hasanean, H.; Almazroui, M. Rainfall: Features and Variations over Saudi Arabia, A Review. *Climate* **2015**, *3*, 578–626. [[CrossRef](#)]
2. Subyani, A.M. Geostatistical study of annual and seasonal mean rainfall patterns in southwest Saudi Arabia/Distribution géostatistique de la pluie moyenne annuelle et saisonnière dans le Sud-Ouest de l'Arabie Saoudite. *Hydrol. Sci. J.* **2004**, *49*, 817. [[CrossRef](#)]
3. Almazroui, M. Dynamical downscaling of rainfall and temperature over the Arabian Peninsula using RegCM4. *Clim. Res.* **2012**, *52*, 49–62. [[CrossRef](#)]
4. Almazroui, M.; Islam, M.N.; Jones, P.D.; Athar, H.; Rahman, M.A. Recent climate change in the Arabian Peninsula: Seasonal rainfall and temperature climatology of Saudi Arabia for 1979–2009. *Atmos. Res.* **2012**, *2012*, 29–45. [[CrossRef](#)]
5. AlSarmi, S.; Washington, R. Recent observed climate change over the Arabian Peninsula. *J. Geophys. Res. Atmos.* **2011**, *116*, D11109. [[CrossRef](#)]
6. Barth, H.-J.; Steinkohl, F. Origin of winter precipitation in the central coastal lowlands of Saudi Arabia. *J. Arid. Environ.* **2004**, *57*, 101–115. [[CrossRef](#)]
7. Mahmoud, M.T.; Mohammed, S.A.; Hamouda, M.A.; Mohamed, M.M. Impact of Topography and Rainfall Intensity on the Accuracy of IMERG Precipitation Estimates in an Arid Region. *Remote Sens.* **2021**, *13*, 13. [[CrossRef](#)]
8. Almazroui, M. Rainfall Trends and Extremes in Saudi Arabia in Recent Decades. *Atmosphere* **2020**, *11*, 964. [[CrossRef](#)]
9. Chowdhury, S.; Al-Zahrani, M. Implications of Climate Change on Water Resources in Saudi Arabia. *Arab. J. Sci. Eng.* **2013**, *38*, 1959–1971. [[CrossRef](#)]

10. Patlakas, P.; Stathopoulos, C.; Flocas, H.; Kalogeri, C.; Kallos, G. Regional Climatic Features of the Arabian Peninsula. *Atmosphere* **2019**, *10*, 220. [[CrossRef](#)]
11. Dupont, B.; Allen, D.L. *Revision of the Rainfall-Intensity Duration Curves for the Commonwealth of Kentucky*; University of Kentucky Transportation Center: Lexington, KY, USA, 1999.
12. Sun, Y.; Wendi, D.; Kim, D.E.; Liong, S.-Y. Deriving intensity–duration–frequency (IDF) curves using downscaled in situ rainfall assimilated with remote sensing data. *Geosci. Lett.* **2019**, *6*, 17. [[CrossRef](#)]
13. Keifer, C.; Chu, H.H. Synthetic Storm Pattern for Drainage Design. *J. Hydraul. Eng.* **1957**, *83*, 1–25.
14. Koutsoyiannis, D.; Kozonis, D.; Manetas, A. A mathematical framework for studying rainfall intensity-duration-frequency relationships. *J. Hydrol.* **1998**, *206*, 118–135. [[CrossRef](#)]
15. Cook, N.J. *Designers Guide to Wind Loading of Building Structures. Part 1*; Butterworth Publishers: Stoneham, MA, USA, 1986; p. 352.
16. Palutikof, J.P.; Brabson, B.B.; Lister, D.H.; Adcock, S.T. A review of methods to calculate extreme wind speeds. *Meteorol. Appl.* **1999**, *6*, 119–132. [[CrossRef](#)]
17. Platon, P.; George, G.; Nicolas, B.; George, K. Extreme wind events in a complex maritime environment: Ways of quantification. *J. Wind. Eng. Ind. Aerodyn.* **2016**, *149*, 89–101. [[CrossRef](#)]
18. Cramér, H. *Mathematical Methods of Statistics*; Princeton University Press: Princeton, NJ, USA, 1946; p. 591.
19. Hazewinkel, M. *Encyclopaedia of Mathematics*; Springer: Dordrecht, The Netherlands, 2000. [[CrossRef](#)]
20. Stergios, E.; Andreas, L.; Efthymios, I.N.; Emmanouil, N.A. Quantitative assessment of annual maxima, peaks-over-threshold and multifractal parametric approaches in estimating intensity-duration-frequency curves from short rainfall records. *J. Hydrol.* **2020**, *589*, 125151. [[CrossRef](#)]
21. Daniel, M.; Efthymios, I.N.; Francesco, M.; Emmanouil, N.A. Precipitation frequency analyses based on radar estimates: An evaluation over the contiguous United States. *J. Hydrol.* **2019**, *573*, 299–310. [[CrossRef](#)]
22. Patlakas, P.; Galanis, G.; Diamantis, D.; Kallos, G. Low wind speed events: Persistence and frequency. *Wind Energy* **2017**, *20*, 1033–1047. [[CrossRef](#)]
23. Daniel, G. Combining regional approach and data extension procedure for assessing GEV distribution of extreme precipitation in Belgium. *J. Hydrol.* **2002**, *268*, 113–126. [[CrossRef](#)]
24. Chow, V.T.; Maidment, D.R.; Mays, L.W. *Applied Hydrology*; McGraw-Hill: New York, NY, USA, 1988.
25. Pielke, R.A.; Cotton, W.R.; Walko, R.L.; Tremback, C.J.; Lyons, W.A.; Grasso, L.D.; Nicholls, M.E.; Moran, M.D.; Wesley, D.A.; Lee, T.J.; et al. A comprehensive meteorological modeling system—RAMS. *Meteorol. Atmos. Phys.* **1992**, *49*, 69–91. [[CrossRef](#)]
26. Cotton, W.R.; Pielke, R.A., Sr.; Walko, R.L.; Liston, G.E.; Tremback, C.J.; Jiang, H.; McAnelly, R.L.; Harrington, J.Y.; Nicholls, M.E.; Carrio, G.G.; et al. RAMS 2001: Current status and future directions. *Meteorol. Atmos. Phys.* **2003**, *82*, 5–29. [[CrossRef](#)]
27. Kallos, G.; Solomos, S.; Kushta, J.; Mitsakou, C.; Spyrou, C.; Bartsotas, N.; Kalogeri, C. Natural and anthropogenic aerosols in the Eastern Mediterranean and Middle East: Possible impacts. *Sci. Total. Environ.* **2014**, *488–489*, 389–397. [[CrossRef](#)]
28. Kushta, J.; Kallos, G.; Astitha, M.; Solomos, S.; Spyrou, C.; Mitsakou, C.; Lelieveld, J. Impact of natural aerosols on atmospheric radiation and consequent feedbacks with the meteorological and photochemical state of the atmosphere. *J. Geophys. Res. Atmos.* **2014**, *119*, 1463–1491. [[CrossRef](#)]
29. Patlakas, P.; Stathopoulos, C.; Tsalis, C.; Kallos, G. Wind and wave extremes associated with tropical-like cyclones in the Mediterranean basin. *Int. J. Climatol.* **2021**, *41*, E1623–E1644. [[CrossRef](#)]
30. Stathopoulos, C.; Patlakas, P.; Tsalis, C.; Kallos, G. The Role of Sea Surface Temperature Forcing in the Life-Cycle of Mediterranean Cyclones. *Remote Sens.* **2020**, *12*, 825. [[CrossRef](#)]
31. Bartsotas, N.S.; Anagnostou, E.N.; Nikolopoulos, E.I.; Kallos, G. Investigating Satellite Precipitation Uncertainty Over Complex Terrain. *J. Geophys. Res. Atmos.* **2018**, *123*, 5346–5359. [[CrossRef](#)]
32. Dee, D.P.; Uppala, S.M.; Simmons, A.J.; Berrisford, P.; Poli, P.; Kobayashi, S.; Andrae, U.; Balmaseda, M.A.; Balsamo, G.; Bauer, P.; et al. The ERA-Interim reanalysis: Configuration and performance of the data assimilation system. *Q. J. R. Meteorol. Soc.* **2011**, *137*, 553–597. [[CrossRef](#)]
33. Thiébaux, J.; Rogers, E.; Wang, W.; Katz, B. A New High-Resolution Blended Real-Time Global Sea Surface Temperature Analysis. *Bull. Am. Meteorol. Soc.* **2003**, *84*, 645–656. [[CrossRef](#)]
34. Olson, J.S. *Global Ecosystem Framework—Definitions*; USGS EROS Data Center Internal Report: Sioux Falls, SD, USA, 1994; 37p.
35. Olson, J.S. *Global Ecosystem Framework—Translation Strategy*; USGS EROS Data Center Internal Report: Sioux Falls, SD, USA, 1994; 39p.
36. Defries, R.S.; Townshend, J.R.G. NDVI-derived land cover classifications at a global scale. *Int. J. Remote Sens.* **1994**, *15*, 3567–3586. [[CrossRef](#)]
37. Wilks, D.S. *Statistical Methods in the Atmospheric Sciences (International Geophysics Series; v. 91)*; Academic Press: Cambridge, MA, USA, 2006; ISBN1 13: 978-0-12-751966-1. ISBN2 10: 0-12-751966-1.
38. Huffman, G.J.; Bolvin, D.T.; Nelkin, E.J.; Wolff, D.B.; Adler, R.F.; Gu, G.; Hong, Y.; Bowman, K.P.; Stocker, E.F. The TRMM Multisatellite Precipitation Analysis (TMPA): Quasi-Global, Multiyear, Combined-Sensor Precipitation Estimates at Fine Scales. *J. Hydrometeorol.* **2007**, *8*, 38–55. [[CrossRef](#)]
39. Tan, J.; Petersen, W.A.; Kirstetter, P.-E.; Tian, Y. Performance of IMERG as a Function of Spatiotemporal Scale. *J. Hydrometeorol.* **2017**, *18*, 307–319. [[CrossRef](#)] [[PubMed](#)]

40. Standards and Recommended Practices. Available online: <https://public.wmo.int/en/resources/standards-technical-regulations> (accessed on 3 June 2021).
41. Abdullah, M.A.; Al-Mazroui, M.A. Climatological study of the southwestern region of Saudi Arabia. I. Rainfall analysis. *Climate Res.* **1998**, *9*, 213–223. [[CrossRef](#)]
42. Mansour, A.; Islam, M.N.; Fahad, S.; Abdulrahman, K.A.; Ramzah, D. Assessing the robustness and uncertainties of projected changes in temperature and precipitation in AR5 Global Climate Models over the Arabian Peninsula. *Atmos. Res.* **2017**, *194*, 202–213. [[CrossRef](#)]
43. AlSarmi, S.H.; Washington, R. Changes in climate extremes in the Arabian Peninsula: Analysis of daily data. *Int. J. Climatol.* **2014**, *34*, 1329–1345. [[CrossRef](#)]
44. Mann, H.B. Nonparametric Tests Against Trend. *Econometrica* **1945**, *13*, 245–259. [[CrossRef](#)]
45. Kendall, M.G. *Rank Correlation Methods*, 4th ed.; Griffin: London, UK, 1975.